Bioactive Wound Dressing based on Decellularized Tendon and GelMA with Incorporation of PDA-loaded Asiaticoside Nanoparticles for Scarless Wound Healing

Shuang Liu[a,e#], Yingsong Zhao[c,#], Ming Li[a,e#], Lei Nie[b,d,*], Qianqian Wei[b], Oseweuba Valentine Okoro[d], Hafez Jafari[d], Siyuan Wang[c], Jun Deng[a], Jianghai Chen[c,*], Amin Shavandi [d,*], and Lihong Fan[a,*]

[a] School of Resources and Environmental Engineering, Wuhan University of Technology, Wuhan 430070, P. R. China

[b] College of Life Sciences, Xinyang Normal University, Xinyang 464000, P. R. China.

[c] Wuhan Union Hospital, Tongji Medical College, Huazhong University of Science and Technology (HUST), Wuhan 430077, P. R. China

[d] BioMatter unit - École polytechnique de Bruxelles, Université Libre de Bruxelles, Avenue F.D. Roosevelt, 50 - CP 165/61, 1050 Brussels, Belgium

[e] Hainan Research Institute, Wuhan University of Technology, Wuhan 430070, P. R. China

[#]These authors contributed equally to this work and should be considered co-first authors.

Corresponding Authors

Prof. Lihong Fan:

Post address: School of Resources and Environmental Engineering, Wuhan University of Technology, 122 Luoshi Road, Wuhan, Hubei, 430070, China.

ORCID: 0000-0001-8277-4007. Tel: +86-13018011218

E-mail: Fanlihong2000@163.com

Prof. Lei Nie:

Post address: College of Life Sciences, Xinyang Normal University (XYNU), Xinyang 464000, China. Tel: +86-13600621068.

ORCID: 0000-0002-6175-5883

E-mail address: nieleifu@yahoo.com; nielei@xynu.edu.cn

Prof. Amin Shavandi

Post address: BioMatter unit - École polytechnique de Bruxelles, Université Libre de Bruxelles, Avenue F.D. Roosevelt, 50 - CP 165/61, 1050 Brussels, Belgium

E-mail address: amin.shavandi@ulb.be

Prof. Jianghai Chen

Post address: Wuhan Union Hospital, Tongji Medical College, Huazhong University of Science and Technology (HUST), 1277 Jiefang Road, Wuhan, Hubei, 430070, China.

E-mail address: chenjianghai@hust.edu.cn

Abstract

In this study, bioactive composite hydrogels were created using the decellularized extracellular matrix (ECM), GelMA, and Polydopamine-loaded Asiaticoside (AC@PDA) nanoparticles for use as wound dressings that could promote healing ~~and prevent infection~~. A decellularization method was used to obtain ECM from porcine Achilles tendon tissue. AC@PDA nanoparticles were then synthesized and found to have a uniform spherical structure with good cytocompatibility, particularly when compared to PDA nanoparticles alone. The mechanical properties of the bioactive composite hydrogels showed good elasticity and shape recovery after compression, with a slight decrease in compressive strength due to the addition of nanoparticles. The formation of interpenetrating networks through the use of EDC/NHS was also found to improve the mechanical properties and moisture retention of the hydrogels. The PDA/ECM-G and AC@PDA/ECM-G hydrogels showed higher water absorption capacity and similar moist retention capacity to the ECM-G hydrogel. The microstructure of the hydrogels was observed through SEM, with the ECM-G hydrogel showing a dense and compact structure, while the PDA/ECM-G and AC@PDA/ECM-G hydrogels displayed a more porous and interconnected structure due to the presence of nanoparticles. In vitro cytotoxicity tests on human skin fibroblasts showed good biocompatibility for all hydrogels. The *in vivo* wound healing performance of the hydrogels was also tested on a full-thickness excisional wound model in mice, with the AC@PDA/ECM-G hydrogel showing the fastest wound closure without scarring and the highest-formed hair follicles. The

AC@PDA/ECM-G hydrogel had the best performance in promoting wound healing. These results suggest that the bioactive hydrogel has the potential for use as a wound dressing.

Keywords

Bioactive hydrogels, extracellular matrix, wound dressing, scarless wound healing.

1. Introduction

Skin is the largest organ of the human body and serves as an essential barrier to provide protection against microorganism infiltration and dehydration. The skin is extremely vulnerable to injury, and the skin defects over a certain diameter cannot heal spontaneously, though the human skin possesses high self-regeneration potentials [1, 2]. Wound healing is a dynamic and complex process, and the regeneration of wounds includes four continuous stages, that is, hemostasis, inflammation, proliferation, and remodeling [3]. Acute and/or chronic wounds impose a notable burden on patients and healthcare systems all over the world. Appropriate wound dressing treatment strategies could alleviate this costly burden, such as gauze, foams, hydrogels, and others [4, 5]. Hydrogels are considered the most competitive wound dressings due to their good tissue compatibility, good hydrophilicity, hygroscopicity, moisture retention, and three-dimensional (3D) porous structure [6]. Hydrogels consist of around 90 wt% water and 10 wt% natural or/and synthetic polymers formed through both covalent and supramolecular non-covalent interactions [1, 7]. Mao *et al.*, [8] fabricated a series of multifunctional nanocomposite hydrogels using bacterial cellulose (BC), gelatin, and selenium nanoparticles. The prepared hydrogels exhibited remarkable antibacterial, antioxidative and anti-inflammatory abilities. In addition, the rat full-thickness defect model confirmed the excellent skin wound healing performance of the prepared hydrogels via the notably enhanced wound closure and angiogenesis.

The wound-healing process could be significantly improved using bioactive

hydrogels, which are able to stimulate cell migration, proliferation, and differentiation and enhance blood vessel formation [9]. Currently, bioactive hydrogels are mainly fabricated by incorporation of growth factors; however, such a strategy still faces clinical application challenges [9-11]. The decellularized extracellular matrix (ECM) hydrogels, as bioactive hydrogels, could retain the structural characteristics and stimulatory properties of the hydrogels and can also enhance the growth, migration, proliferation, differentiation, and angiogenesis of the seed cells [12, 13]. Generally, decellularized ECMs could be harvested from natural mammalian tissue sources by removing cells and DNA content, and a large variety of macromolecules contribute to the ECM structure and function, including fibrous ECM proteins, proteoglycans (PGs), and glycosaminoglycans (GAGs) [14-16]. Zhao *et al.*, [17] obtained decellularized ECM from a porcine Achilles tendon myotendinous junction and generated a scaffold using decellularized ECM with a well-preserved native biphasic layered hierarchical structure, biological composition, and excellent mechanical properties. The fabricated ECM scaffold displayed minimal immunological reaction. Some researches confirmed that ECM-derived hydrogel had a positive influence on tissue regeneration due to that it could trigger the release of some bioactive molecules, such as vascular endothelial growth factor (VEGF) and insulin-like growth factor (IGF), and activate stem cells to promote vascularization and new tissue formation [18, 19]. Ryzhuk *et al.*, [20] developed a cost-effective method to produce bioactive ECM-derived hydrogel from easily accessible human amniotic membranes. The results demonstrated that the hydrogel is biocompatible with a wide range of stem cell types and is promising for

tissue repair and regeneration. The decellularized ECM has the function of acting as a biological platform to correctly interact cells and biomolecules, and reconstructing cutaneous lesions by providing the required functional domains for cell differentiation in wound healing [21]. Lin *et al.*, [22] obtained acellular dermal matrix (ADM) from mouse skin and designed chitosan/ADM scaffold, which provides a protective environment for mesenchymal stem cells (MSCs) survival in vivo and contributes to the growth of vessel and the acceleration of wound healing. Also, Bankoti *et al.*, [23] fabricated bioactive hydrogel with the extracted ADM using a dual cross-linking approach with ionic crosslinked with chitosan and covalent crosslinked using iodine-modified 2,5-dihydro-2,5-dimethoxy-furan, and the bioactive hydrogel treated full thickness burn wounds and demonstrated rapid healing.

However, scarring in the skin still presents a significant medical problem, which leads to restriction of movement, loss of tissue function, and severe psychological morbidities [24]. The development of scarless wound hydrogel dressing is still urgently needed and challenging. Transforming growth factor-β (TGF-β) signalling has been well-recognized as a key regulator of skin wound repair. However, the dysregulation of TGF-β signalling contributes to pathological skin scarring [25]. Zhang *et al.*, [26] integrated a photo-crosslinking strategy and a microcapsule platform to develop wound dressing materials for the pulsatile release of TGF-β, and the skin wound closure was greatly enhanced with effectively suppressing scar formation. Asiaticoside (AC) is a triterpenoid compound extracted from *Centella asiatica*, which has been used as a Chinese herbal medicine for thousands of years

[27]. Many reports have confirmed that AC demonstrates the outstanding functions of anti-ulcer, anti-inflammatory, anti-depression, anti-dementia, antibacterial and antioxidant activities [28, 29]. AC plays an important role to support wound healing through its multiple mechanisms and activities, includes reducing wound oxidation, stimulating collagen synthesis, accelerating cell proliferation, promoting angiogenesis, changing the secretion and arrangement of collagen fibers, and inhibiting scar growth [30-33]. However, the poor solubility and lipophilicity of AC limit its pharmacological and therapeutic potential in wound healing [31, 34, 35]. So, an effective delivery system is required to deliver AC to wounded skin. Liu *et al.,* [36] designed the AC-loaded silk nanofiber hydrogels as bioactive and injectable matrices for skin regeneration. After the implantation of prepared AC-laden hydrogel matrices to the full-thickness wound defects in rats, scarless wound repair was achieved, and inflammatory reactions and angiogenesis were regulated during the inflammation and remodeling stages.

In the present research work, the decellularized ECM was prepared from porcine tendon using a new decellularization technology. Next, GelMA was composited with prepared decellularized ECM and crosslinked using EDC/NHS, and AC-loaded polydopamine (PDA) nanoparticles were incorporated to obtain the bioactive hydrogel (**Scheme 1**). The physiologically relevant properties of the bioactive hydrogel, such as the rheological properties, mechanical strength, and microstructure, were characterized. The biocompatibility and wound healing efficacy were evaluated in vitro and in vivo. Furthermore, the mechanism of the bioactive hydrogel for

158 scarless wound healing was discussed through tissue section staining and
159 histochemical analysis.
160
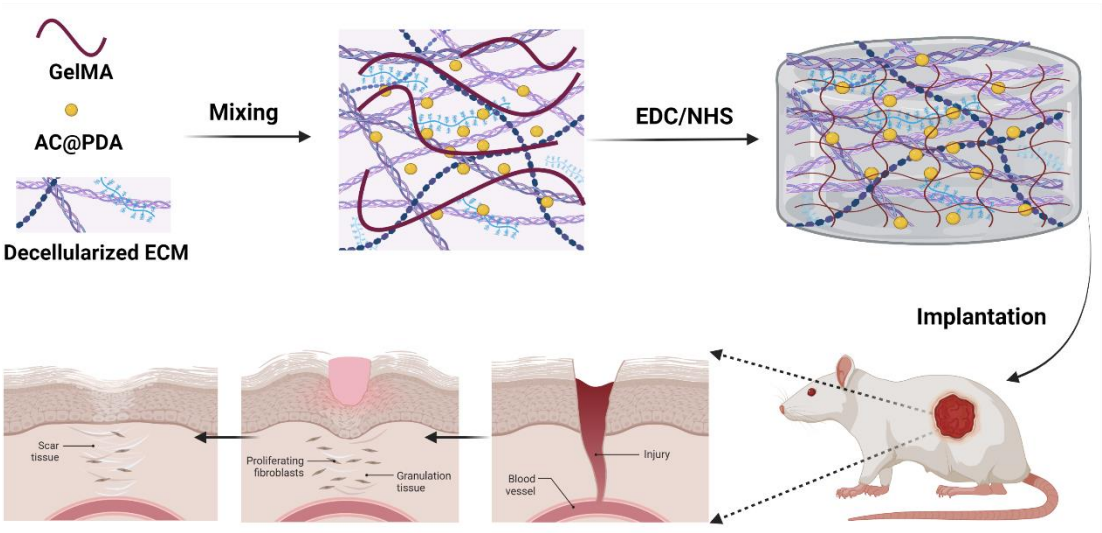

161
162 **Scheme 1**. Schematic illustration of the fabrication of bioactive hydrogels as wound dressing
163 using decellularization ECM, GelMA, and PDA-loaded AC nanoparticles for skin regeneration.
164
165 ## 2. Materials and Methods
166 ### 2.1 Chemicals and Materials
167 Gelatin (Gel, Catalog Number: 10010326), sodium hydroxide (NaOH), acetic
168 acid (CH_3COOH, HAc), and hydrochloric acid (HCl) were purchased from
169 Sinopharm Chemical Reagents Co., Ltd. Fresh porcine tendon was purchased from
170 Wuchang Slaughterhouse (Wuhan, China). Phosphate buffer salt (PBS), sodium
171 dodecyl sulfate ($CH_3(CH_2)_{11}OSO_3Na$, SDS), N-hydroxysuccinimide (NHS),
172 dopamine (DA), 1-ethy-3-(3-dimethylaminopropyl carbodiimide) hydrochloride
173 (EDC), and methacrylic anhydride ($C_8H_{10}O_3$) were purchased from Aladdin Co., Ltd.
174 Asiaticoside ($C_{48}H_{78}O_{19}$, AC) was purchased from Best-reagent Co., Ltd. Triton X-

100 was obtained from Amresco Co., Ltd. All reagents were purchased and used directly without further purification.

2.2 Preparation of Decellularized Extracellular Matrix (ECM)

The decellularized extracellular matrix (ECM) was prepared according to the previous modified methods [37, 38]. The fresh porcine tendon tissues were cut into 0.5 cm × 0.5 cm slices and washed using PBS for 2 h. The sliced tissues were soaked in a 0.5 % SDS and 0.5 % Triton X-100 and stirred for 24 h. After then, the soaked tissues were washed thoroughly using PBS again. Next, the tissues were treated with 1 % HAc solution for 24 h and washed using distilled water for 48 h. Lastly, the tissues were freeze-dried and milled to powder using a grinding miller, and the obtained powder was added to distilled water to obtain ECM samples (0.6 %, 0.8 % and 1 %), and the samples were frozen and stored.

2.3 Synthesis of Polydopamine-loaded Asiaticoside (AC@PDA) Nanoparticles

180 mg of DA powder was dissolved in 90 mL of Millipore water, and the pH of the solution was adjusted to 8.5 using 1 M NaOH solution, and stirred for 24 h at 25 °C, and the solution was centrifuged (4000 r/min) for 15 min to obtain the black precipitated powder, and the powder was washed using Millipore water 5 times to remove residual NaOH, and freeze-dried to obtain black PDA nanoparticles powder. Next, 0.2 mg of lyophilized PDA nanoparticles powder was added into 10 mL of methanol solution (20 ug/mL) , and treated ultrasonically for 2 h at 4 °C. The mixed solution was freeze-dried to obtain AC@PDA nanoparticles and stored at 4 °C.

2.4 Synthesis of Methacrylate Gelatin (GelMA)

GelMA was prepared according to the previous literature [39, 40]. Briefly, 50 mL of gelatin solution (10 w/v %) was mixed with 5 mL of methacrylate anhydride (20 w/v %). The mixed solution was stirred (600 r/min) for 2 h. Then, the reaction was stopped using 5-fold diluted PBS and dialyzed in distilled water for one week at 40 °C in a 12–14 kDa dialysis bag. Afterwards, the treated solution was freeze-dried to obtain GelMA and stored at –80 °C.

2.5 Preparation of Bioactive Composite Hydrogels

8 g of obtained ECM (0.8 wt%) and 8 g of GelMA (10 wt%) were mixed in a beaker (50 mL), and stirred (600 r/min) for 6 h at 37 °C to obtain a uniform solution. Then, 2 mg of AC@PDA nanoparticles was added to the above solution and stirred (800 r/min) for 2 h at 37 °C. After then, EDC (50 mM) and NHS (25 mM) were added to the above solution, stirred (1000 r/min) for 20 min at 37 °C, and stilled for 1 h to obtain bioactive composite hydrogel, and the obtained hydrogel was designated as AC@PDA/ECM-G (**Scheme 1**). At the same time, the composite hydrogel based on ECM and GelMA using the same method was fabricated and designated as ECM-G, and the composite hydrogel based on ECM, GelMA, and PDA nanoparticles using the same method was prepared and designated as PDA/ECM-G.

2.6 Fourier Infrared Spectroscopy (FT-IR) Analysis

The presence of specific chemical groups in prepared samples was analyzed using the Attenuated Total Reflectance-Fourier Transform Infrared Spectroscopy (ATR-FTIR, ThermoFisher, Nicolelis5). The FTIR spectra were obtained within the range between 500 and 4000 cm^{-1} with a resolution of 1 cm^{-1}, with 64 scans for each

spectrum.

2.7 Ultraviolet-visible Spectroscopy (UV-vis) Analysis

Ultraviolet–visible Spectroscopy (UV–Vis, PerkinElmer, Lambda 950) was used to investigate the diffuse reflectance spectra of samples. The sample was operated in the range of 200–800 nm at 298 K.

2.8 Dynamic Light Scattering (DLS) Analysis

The size distribution of PDA and AC@PDA nanoparticles was examined by Dynamic Light Scattering (DLS, Malvern Zetasizer 3000E).

2.9 Transmission Electron Microscopy (TEM) Analysis

The morphology of PDA and AC@PDA nanoparticles was examined by Transmission Electron Microscope (TEM, Tecnai G2 F20). The PDA and AC@PDA nanoparticles were dispersed in Millipore water and sonicated for 2 h. After then, the copper grid was dipped into the prepared solutions and dried under infrared lamp for TEM test.

2.10 Scanning Electron Microscope (SEM) Analysis

The microstructure of hydrogels was observed under Cold Field Scanning Electron Microscopy (SEM, S-4800, Hitachi). The hydrogels were freeze-dried and cut into thin slices, and adhered on the SEM scaffold using a conductive glue. Then, the surface of the samples was sprayed with a thin platinum conductive layer for SEM test.

2.11 Compressive Strength Analysis

The compression strength of the prepared hydrogels was investigated by using an

electromechanical universal testing machine (CMT4103, China) at a crosshead contraction speed of 2 mm/minute. The secondary cyclic compressive stress-strain curves of hydrogels were recorded (deformation 95%).

2.12 Rheological Test

The rheological properties of the prepared hydrogels were evaluated using a DHR-2 rheometer (TA, USA). The test was carried out using a 40 mm diameter and 1 mm clearance aluminium low inertia parallel plate, and the edge of the fixture was sealed using glycerin to avoid water evaporation from the sample during the test. The energy storage modulus (G') and loss modulus (G") of hydrogels were measured by varying the temperature and frequency.

2.13 Water Absorption and Moisture Retention Performance

The mass of each freeze-dried hydrogel was recorded initially as m_1, and the sample was inserted in distilled water for 24 h to reach saturation. Then, the swollen hydrogel was taken out, and the water on the surface of the sample was wiped off. The mass of the sample was recorded as m_2. The water evaporation rate (*WER*) of the hydrogel was then calculated as follows;

$$\mathrm{WER} = \frac{m_2 - m_1}{m_1} \times 100\%$$

The saturated hydrogel at the equilibrium state was placed in an oven at 37 °C for 48 h, and then the mass of samples was recorded as m_3. The moisture retention (*MR*) of the hydrogel was calculated as follows;

$$\mathrm{MR} = \frac{m_3}{m_2} \times 100\%$$

2.14 Biodegradation Evaluation

The freeze-dried hydrogel was soaked in simulated body fluid (SBF) for 24 h to reach saturation, and the mass was recorded initially as m_0. Then, the swollen sample hydrogel was immersed in SBF and placed in a shaker at 37 °C (100 rpm/min). All samples were sealed without refreshing SBF to minimize pH changes and microbial contamination. The sample was taken out at the predesignated time, and the water on the surface of the sample was wiped off, the mass was recorded as m_t. The *in vitro* biodegradation rate (*DD*) of the hydrogel in SBF was then calculated as follows;

$$DD = \left(1 - \frac{m_0 - m_t}{m_0}\right) \times 100\%$$

2.15 Free Radical Scavenging Rate Test

The free radical (·OH) scavenging rate of the prepared hydrogels was tested according to the method described in the literature [41, 42]. Briefly, 1.0 mL of the sample was mixed with 1.0 mL of 1,10-phenanthroline solution (1.5 mmol/L), then 1.0 mL of hydrogen peroxide solution (0.03 %) was added and reacted for 1 h at 37 °C. The absorbance of the complex solution at 536 nm was measured using an ultraviolet spectrophotometer and recorded as A_t. At the same time, the test sample was replaced by 1.0 mL of distilled water and considered as the control group, and its absorbance was recorded as A_n. Also, the hydrogen peroxide was replaced by distilled water and considered as the blank group, and its absorbance was recorded as A_b. The hydroxyl radical scavenging rate was subsequently calculated as follows;

$$^{\bullet}\mathrm{OH} = \frac{A_t - A_n}{A_b - A_n} \times 100\%$$

2.16 Cell Culture

Human skin fibroblasts (HSF, PCS-201-012, ATCC) were used to be cultured

according to ATCC instructions. The HSF cells were cultured in a T25 cell culture flask under a humidified atmosphere of 95 % air and 5 % CO_2 at 37 °C. The cell culture medium (Dulbecco's modified Eagle's medium (DMEM) supplemented with 10 % of fetal bovine serum and 5% of penicillin streptomycin) was replaced every two days. After the cell density reached 80%, cells were digested using trypsin and re-suspended in a new cell medium. The 3rd generation HSF cells were used for the next experiments.

2.17 CCK-8 Analysis

The CCK-8 assay was used to evaluate the cytocompatibility of the prepared hydrogels by culturing them with HSF cells. The hydrogel was cut into a circular disk with a diameter of 8 mm and soaked in ethanol (75 v/v%) for sterilization, and then the samples were washed with sterile PBS. The HSF cells (1×10^4 cells /mL for each sample) were seeded onto hydrogels and cultured for 1, 3, and 5 days in a 48-well plate (Corning). After then, a 10 μL CCK-8 kit solution was added and agitated. The plate was moved in a CO_2 atmosphere for 4 h. The O.D value at 450 nm of each orifice was measured using a microplate reader (SpectraMax 190, USA). Cells cultured without adding hydrogels were used as a blank control group.

2.18 Fluorescence Analysis

The viability of HSF cells was also evaluated using the Calcein acetoxymethylester/propidium iodide (Calcein-AM/PI) Double Stain Kit (Zeye Biotechnology Co., Ltd, Shanghai). Both living and dead cells were stained simultaneously, and living cells produced green fluorescence because of calcein, and

dead cells produced red fluorescence owing to propidium iodide (PI). After hydrogels were cultured with cells on days 1, 3, and 5, glutaraldehyde (2.5 %) was added to localize the cells. Then, the samples were rinsed twice using PBS, and cells were labelled using the Calcein-AM/PI Kit according to the supplier's instruction. The cells were observed under a confocal laser microscope (CLSM, Leica TCS SP5 II, Germany).

2.19 Cell Migration Assay

HSF cells were seeded at the 96-well plate and co-cultured with 100 μL of hydrogel extract at 37 °C for 24 h. After then, the liquid was removed, and a straight line was scratched on the cell monolayer with a 10 μL pipette sharp tip; the wells were washed twice using PBS to remove the damaged cells. Next, 100 μL of fresh medium was added to the wells, and the original straight line was recorded using an optical microscope. Subsequently, the plate was placed in an incubator for 24 h, and the change of scratch straight line was recorded.

2.20 *In vivo* Wound Healing Study

All animals were treated in accordance with the “Principles of Laboratory Animal Care” (NIH publication #85-23, revised 1985). All in vivo animal experiments were approved by the Animal Ethical Committee of Tongji Medical College, Huazhong University of Science and Technology (HUST). The rat models were established according to previous reports [42] [43]. 25 Sprague Dawley (SD) rats (280 ± 50 g) were divided into 5 groups (*i.e.*, 5 rats in each group). The SD rats were anaesthetized using pentobarbital sodium (3 %, 20 mg/kg). After then, a circular

wound model with a diameter of 15 mm in the middle back of the rat was made, and all epidermis and dermis were removed. Next, the wound sites were treated using GelMA, ECM-G, PDA/ECM-G, and AC@PDA/ECM-G hydrogels, respectively, and physiological saline was used as the control group. Then, the wound was bandaged using gauze, and pictures were captured on days 5, 10 and 15 to observe the wound healing. The wound healing time has been determined by visual observation.

2.21 Histological evaluation

Tissues were collected from the wounds of the above-mentioned rats on day 5, 10 and 15, respectively, and stored at -20 °C, and then the tissues were sectioned and investigated using hematoxylin-eosin (HE) and Masson's staining for optical microscopy observation. The histologic examinations were detected per high power field. For the comparison to normal skin, the epithelium cell layer, amounts of the inflammatory cells and fibroblasts for each group on days 5, 10, and 15 (five sections for each day, and five areas were randomly selected for each sample) were counted and scored using 4 scales: 0 = normal, 1 = mild increase, 2 = moderate increase and 3 = marked increase [44]. The newly formed capillary number and dermis (μm) for each group on days 5, 10, and 15 were analyzed by the same statistical method. The number of hair follicles for each group on day 15 was obtained from the whole sections.

2.22 Statistical Analysis

Each experiment is repeated three times. Values were presented as the means of these replicates ± standard error of the mean. Mean values were compared by one-

way analysis of variance (ANOVA) using SPSS.22 statistical software package, LSD method was used for pairwise comparison with statistical significance established when $p < 0.05$.

3. Results and Discussion

3.1 Preparation and Properties of Decellularized ECM

In this paper, the decellularized ECM was obtained using a porcine Achilles tendon, and the treatment process is shown in **Figure 1A**. During the decellularization process, the structure of fibrous tissue was destroyed by the frozen ice crystals, the extracellular membrane was also punctured, and cells were also detached from the original matrix after using the treatment. The porcine Achilles tendon tissue without fat, the tissue after frozen and HAc treatment, and the final crushed tissue were displayed in **Figures 2B i**, **ii**, and **iii**, respectively. The decellularization process is applied to native tissue to remove the constituent cells and obtain ECM. The tendon tissue used in this paper has a low cell content, which is suitable for decellularization treatment [45]. After the decellularization process, the cell number in the tissue was significantly decreased. The cell distribution in untreated tendon and decellularized ECM was investigated using fluorescence assay (DAPI/Phalloidin-FITC) (**Figure 1C**), the cell nucleus was represented by blue color, and the cytoplasm was represented by green color. It was observed that the residual cells were greatly decreased in ECM in comparison to the untreated tendon. The residual cell content was further statistically analyzed, shown in **Figure 1D**. The cell content in untreated tendon was 77.33 ± 8.22 %

per/mm, and cell content in decellularized ECM was decreased to 0.32 ± 0.13% per/mm. The microstructure of the obtained ECM was investigated using SEM (**Figure 1E**), the interconnected porous microstructure morphology was observed, and no residual cells were observed. The native tendon has a unique tissue structure with bundles of collagen fibers aligned along tissue to display crimp structure [46], and such crimp structure was destroyed in this work using the modified decellularization method.

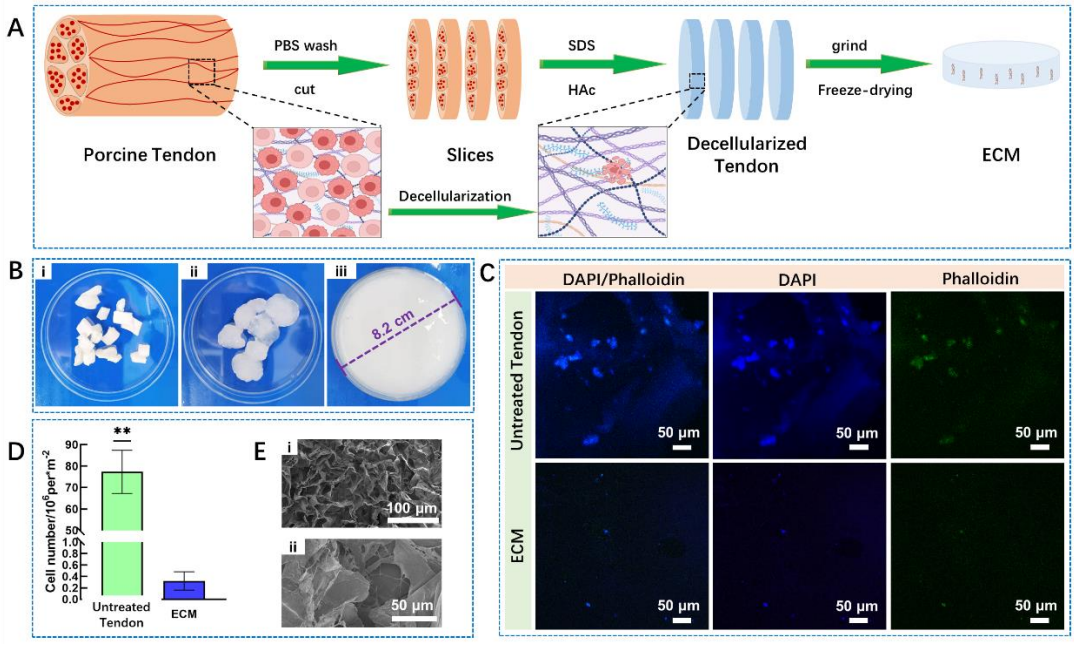

Figure 1. A) Schematic diagram of decellularization process using porcine Achilles tendon. B) The photos showing ECM samples. C) Representative fluorescent microscopy images of prepared ECM and untreated tendon using phalloidin-FITC/DAPI. D) Statistical analysis of residual cells in untreated tendon and obtained ECM, $^{**}p < 0.01$. E) SEM images of the prepared ECM at different magnifications.

3.2 Properties of AC@PDA Nanoparticles

Next, PDA-loaded AC (AC@PDA) nanoparticles were fabricated following the modified literature method [47-49]. PDA nanoparticles were first synthesized using the cyclization and polymerization of monomer dopamine, and then AC was loaded in PDA nanoparticles. The preparation process is shown in **Figure 2A**. FT-IR spectroscopy was performed to confirm the synthesis of PDA nanoparticles, shown in Figure 2B. The peak at 1629 cm^{-1} attributed to the C=O bonds from PDA, and the absorption peak at 2811 cm^{-1} corresponded to the stretching vibration of N-H groups disappeared, and the peak around 3300 cm^{-1} significantly enhanced, confirming the successful synthesis of PDA nanoparticles [50]. The TEM images (**Figures 2C** and **2D**) showed that the obtained PDA and AC@PDA nanoparticles were successfully formed with a uniform spherical structure. The prepared PDA and AC@PDA nanoparticles were monodispersed with an average size of 379.2 ± 14.5 nm and 392.4 ± 17.5 nm, respectively. However, according to the hydrodynamic diameter histogram distribution profile (**Figures 2Cii** and **2Dii**), the hydrodynamic diameter of both PDA and AC@PDA nanoparticles was slightly increased to 481.6 ± 16.3 nm and 563.1 ± 18.2 nm, respectively, whereas the polydispersity index of both nanoparticles was in the range of 0.2. The larger value obtained from the DLS test over TEM images was attributed to the swelling of PDA nanoparticles hydrated in an aqueous solution because of their hydrophilicity [49]. Furthermore, the cytocompatibility of both PDA and AC@PDA nanoparticles was further investigated by culturing with Human skin fibroblasts (HSF) cells (**Figure 2E**). The results showed that both nanoparticles had

good cytocompatibility; however, AC@PDA nanoparticles displayed better cytocompatibility than PDA nanoparticles due to the addition of AC.

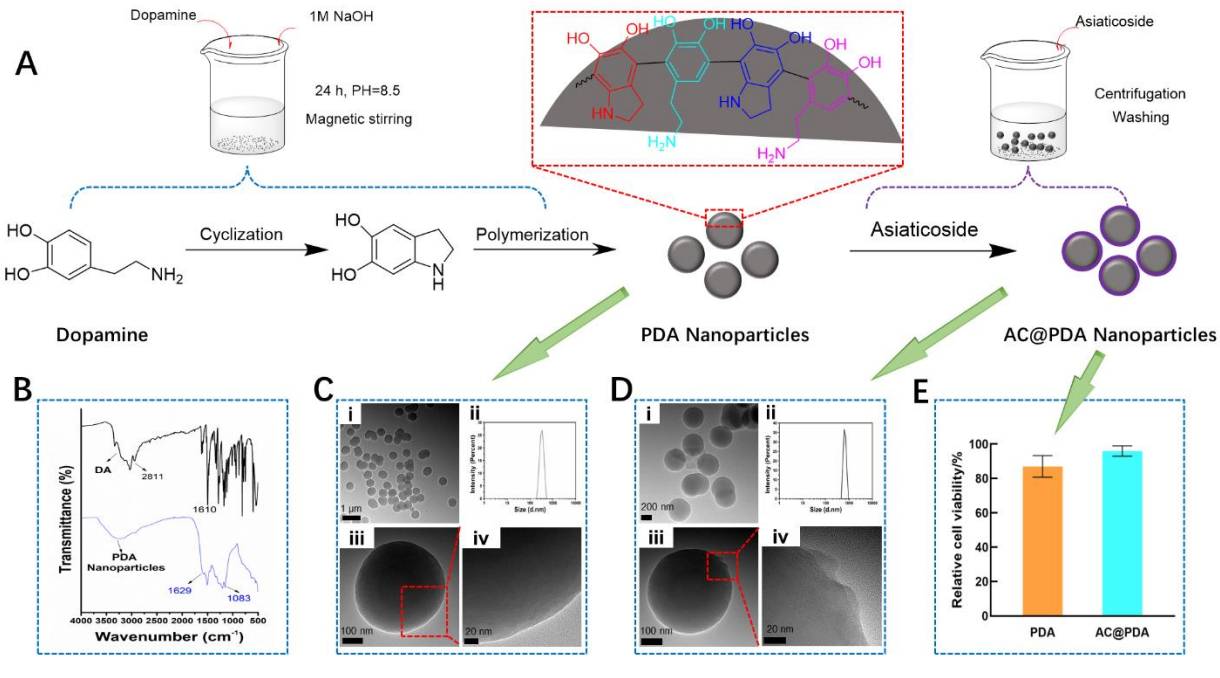

Figure 2. A) Schematic diagram of the fabrication of AC@PDA nanoparticles. B) FT-IR spectra of dopamine (DA) and PDA nanoparticles. C) TEM images (i, iii, iv) and DLS analysis (ii) of PDA nanoparticles. D) TEM images (i, iii, iv) and DLS analysis (ii) of AC@PDA nanoparticles. D) Relative cell viability of HSF culturing with PDA and AC@PDA nanoparticles for 24 h.

3.3 Physiochemical Properties of Bioactive Composite Hydrogels

The bioactive composite hydrogels using decellularized ECM, GelMA, and AC@PDA nanoparticles were fabricated, and the physiochemical properties of hydrogels were investigated, including mechanical properties, water absorption and water retention properties, radical scavenging rate, rheological properties, biodegradability, and microstructure. The successful incorporation of PDA

nanoparticles in hydrogel networks was confirmed using UV-Vis spectrum analysis, and the UV-Vis spectra of all obtained hydrogels are displayed in **Figure 3A**. Compared to ECM-G hydrogel, the absorption peak at 281.50 nm for PDA/ECM-G and AC@PDA/ECM-G hydrogels was observed, mainly due to the absorption of PDA nanoparticles. Furthermore, the detected absorption peak at 346.76 nm for AC@PDA/ECM-G hydrogel was attributed to the characteristic absorption of AC, confirming that successful loading of AC in prepared bioactive AC@PDA/ECM-G hydrogel. The mechanical properties of the obtained bioactive hydrogels were carried out, shown in **Figures 3B** and **3C**. The prepared ECM-G, PDA/ECM-G, and AC@PDA/ECM-G hydrogels are shape re-coverable after compression in the air. The structure of traditional decellularized ECM collapses rapidly after contact with water due to the collapse of pore struts, and then the wound moistness is further influenced [51]. The secondary cyclic compressive stress-strain curves displayed that the bioactive hydrogels had good elasticity, and the compressive strength was not significantly changed after the shaper re-covering. However, there was a slight decrease in the compressive strength for PDA/ECM-G and AC@PDA/ECM-G hydrogels in comparison to that of ECM-G hydrogel due to the addition of nanoparticles. The FT-IR was further used to investigate the obtained hydrogels as shown in **Figure 3D**. The peaks at 3075 and 1654 cm^{-1} contributed to N-H stretching and amide I, respectively, for GelMA hydrogel. For the FT-IR spectrum of ECM-based hydrogels (ECM-G, PDA/ECM-G, and AC@PDA/ECM-G), the typical amide bands at 3086, 1655, and 1552 cm^{-1} could be observed, indicating stretching vibration

of N-H (Amide B), C=O stretching (Amide I), and N-H deformation (Amide II), confirming the existence of collagen proteins in prepared bioactive hydrogels [52]. In addition, the peak at 1067 cm-1 ascribed to olefin moiety from AC was observed in the FT-IR spectrum of AC@PDA/ECM-G hydrogels [53]. EDC, in conjunction with NHS, has the high coupling efficiency to create stable amine-reactive intermediates between ECM and GelMA, and the formed interpenetrating networks in bioactive hydrogels could improve their mechanical properties and moist retention ability [54, 55].

The hydrogels as wound dressings should have the properties of absorbing wound exudate and providing a moist environment to promote wound healing and avoid wound infection [56]. Next, the water absorption and water retention of the bioactive hydrogels were investigated. Compared to ECM-G hydrogel (15.52 ± 6.98 g/g), PDA/ECM-G (34.29 ± 4.93 g/g) and AC@PDA/ECM-G (41.22 ± 10.18 g/g) hydrogels displayed higher values on water absorption capacity (**Figure 3E**). The network of hydrogels enlarges in the presence of PDA or AC@PDA nanoparticles, and the water absorption capacity is greatly improved. The nanoparticles embedded in the hydrogels led to the expansion of the network, and the hydration degree was further significantly increased due to the surface charge of the colloidal nanoparticles [57]. All obtained hydrogels reached the equilibrium of water absorption within around 2 h, then retained the large volumes of water to provide a moist environment for wounds [56]. The moist retention ability of the obtained bioactive hydrogels was further investigated by measuring weight changes of swollen hydrogels at 37 °C after

48 h. ECM-G, PDA/ECM-G, and AC@PDA/ECM-G hydrogels had similar moist retention capacities, and the moist retention ratio of all hydrogels was above 80 %, indicating that the bioactive hydrogels can be effective as wound dressings (**Figure 3F**). The hydroxyl radical scavenging rate is an important index to evaluate the oxidation resistance, and the scavenging ability of the prepared hydrogels was investigated (**Figure 3G**). AC@PDA/ECM-G presented the highest scavenging ability with a scavenging rate of 41.50 ± 3.02 %, in comparison to ECM-G hydrogel (5.22 ± 0.66 %) and PDA/ECM-G hydrogel (11.44 ± 1.05 %). AC had profound free radical scavenging activity. The addition of AC in hydrogels could significantly improve the antioxidant capacities, which had a positive effect on promoting wound healing [58].

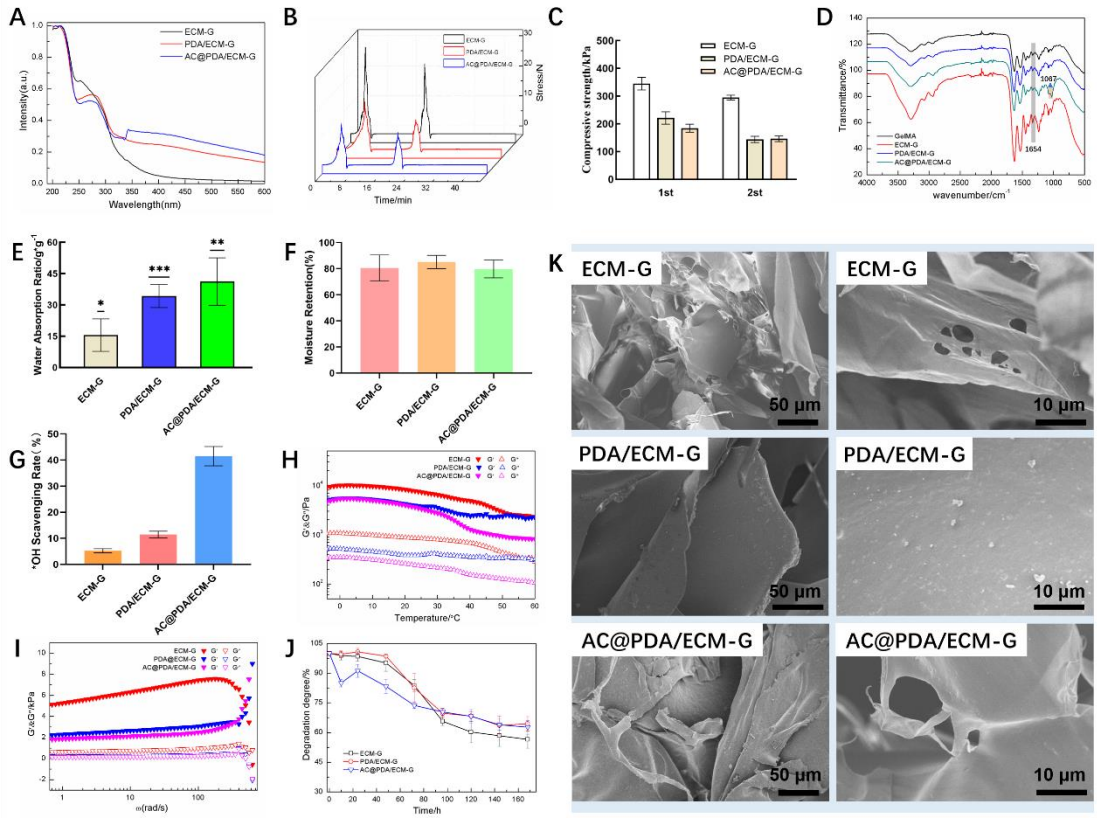

Figure 3. A) UV-Vis spectra of the prepared hydrogels. B) Compressive strength and C) secondary cyclic compressive stress-strain curves of prepared hydrogels. D) FT-IR spectra of

prepared hydrogels. E) Water absorption ration of ECM-G, PDA/ECM-G, and AC@PDA/ECM-G hydrogels. $^{*}p < 0.05$, $^{**}p < 0.01$, $^{***}p < 0.001$. F) Moisture retention and G) hydrogen hydroxyl radicals scavenging ability of the prepared hydrogels. The storage modulus (G') and loss modulus (G'') of hydrogels were evaluated over (H) temperature and (I) frequency. J) In vitro degradation degree of the prepared hydrogels. K) SEM images of ECM-G, PDA/ECM-G, and AC@PDA/ECM-G hydrogels at different magnifications.

Next, the rheological properties of hydrogels were further investigated, and the storage moduli (G') and loss moduli (G'') of hydrogels were tested in terms of temperature and frequency (**Figures 3H** and **3I**). The results show that G' of all obtained hydrogels is greater than G'', exhibiting the typical viscous flow characteristics of hydrogel [39, 59, 60]. There was a slight increase in both G' and G'' with the increase of temperature from -4 °C to 60 °C. With the addition of PDA nanoparticles, both G' and G'' of the hydrogels were decreased mainly due to the fact that the microstructure of the hydrogels could be changed by adding nanoparticles. Both G' and G'' of PDA/ECM-G and AC@PDA/ECM-G hydrogels remain constant in a wide range of angular frequencies. Also, G' of ECM-G hydrogel was greater than that of PDA/ECM-G and AC@PDA/ECM-G hydrogels and increased with increasing angular frequency at first and greatly decreased at high angular frequency. However, G' of PDA/ECM-G and AC@PDA/ECM-G hydrogels significantly increased at high angular frequency, mainly due to the electrostatic force between nanoparticles and hydrogels.

The wound dressings for the chronic wound, bleeding, and deep fissured wounds on the skin surface require degradability necessarily. However, the short-term degradation of wound dressings will lead to the risk of infection after wound exposure [61]. The *in vitro* degradation of ECM-G, PDA/ECM-G and AC@PDA/ECM-G hydrogels in SBF were investigated, with results shown in **Figure 3J**. The degradation degree of ECM-G, PDA/ECM-G and AC@PDA/ECM-G hydrogels in SBF at day 7 were 43.24 ± 4.38 %, 39.13 ± 3.64 % and 32.57 ± 3.45 %, respectively. The AC@PDA/ECM-G hydrogels exhibited the lowest degradation possibly due to the formation of additional hydrogel bonding between the hydroxyl groups of AC, and the functional groups presented in gelatin backbone, leading to increase the crosslinking density and degradation stability of the hydrogel [62].

The addition of PDA nanoparticles slightly slowed down the degradation of the bioactive hydrogels, and AC@PDA/ECM-G hydrogel displayed the slowest degradation degree. Furthermore, the microstructure of the cross-section of the freeze-dried prepared hydrogels was observed by SEM, as shown in **Figure 3K**. PDA and AC@PDA nanoparticles could be observed in SEM images of PDA/ECM-G and AC@PDA/ECM-G hydrogels, respectively. Compared to pure decellularized ECM microstructure (**Figure 1E**), ECM-G, PDA/ECM-G and AC@PDA/ECM-G hydrogels displayed a tighter pore structure due to the formed interpenetrating networks. All obtained bioactive hydrogels showed a relatively homogeneous and interconnected pore structure, indicating their good structural stability and uniform physical structure, which could provide enough space for cell growth and proliferation [42].

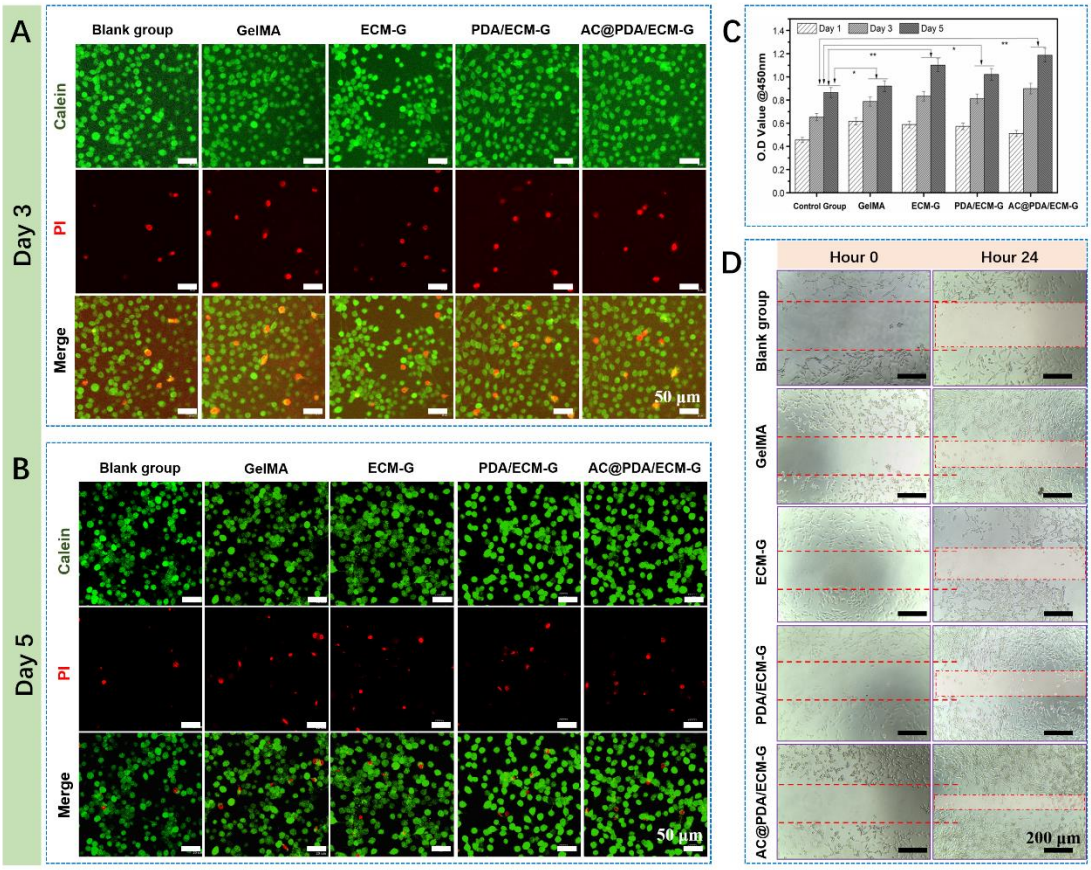

Figure 4. Representative fluorescent microscopy images of prepared ECM-G, PDA/ECM-G, and AC@PDA/ECM-G hydrogels cultured with HSF cells for (A) 3 days and (B) 5 days, and GelMA hydrogels were used as a comparison. Cells without adding samples as a blank group, the hydrogels were stained using Calcein-AM/PI, Scale bar: 50 μm. (C) Cytocompatibility of the prepared hydrogels was evaluated using CCK-8 assay by culturing with HSF cells for 1, 3, and 5 days with the control group, *$p < 0.05$, and **$p < 0.01$. (D) The HSF cells scratch test results for 24 h. All the red dotted lines indicate the width of the scratch gap. Scale bar: 200 μm.

3.4 Cytocompatibility Evaluation

The cytocompatibility of bioactive hydrogels as wound dressings is an important

index for wound healing. The cytocompatibility of the prepared hydrogels was studied using fluorescent analysis and CCK-8 (**Figure 4A-C**). HSF cells were seeded on the ECM-G, PDA/ECM-G, and AC@PDA/ECM-G hydrogels and GelMA hydrogel were used as a comparison, the growths of HSF cells on days 3 and 5 were stained using Calcein acetoxymethylester/propidium iodide (Calcein-AM/PI) and observed using a fluorescent microscope. In the Calcein-AM/PI stained images, live cells were stained green by Calcein-AM, while dead or dying cells were stained red by PI [63]. There were no noticeable morphological abnormalities and no significant differences in the green and red fluorescent images between groups, and plenty of HSF cells were observed for each group on day 3. HSF cells were seeded on the prepared hydrogels and cultured for 1, 3, and 5 days and treated using CCK-8 solution, O.D value at 450 nm was recorded, which indicated the presence of metabolically active cells (**Figure 4C**). According to CCK-8 results, the O.D values of all obtained hydrogels increased over days, confirming their good biocompatibility. AC@PDA/ECM-G hydrogel displayed the highest O.D values on days 3 and 5. The efficiency of wound healing greatly depends upon the migration ability of wound dressing [64]. Furthermore, the pro-migration ability of the prepared bioactive hydrogels was investigated using a scratch assay (**Figure 4D**). Compared to the control group, all prepared hydrogels significantly enhanced HSF cell migration 24 h after scratching. The cell migration ability of AC@PDA/ECM-G hydrogel was higher than that of other groups after 24 h, indicating that the obtained AC@PDA/ECM-G hydrogel could enhance cell migration and accelerate the closure of cell scratches.

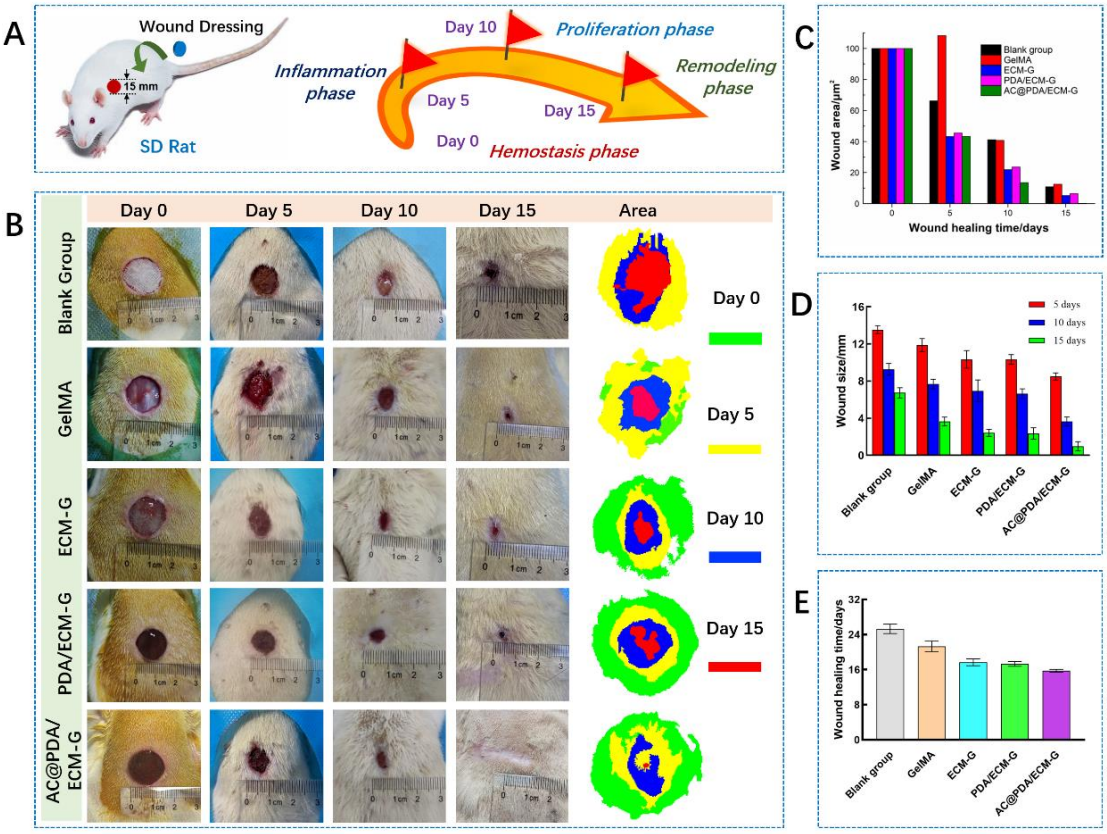

Figure 5. (A) Schematic diagram of SD rat models, the prepared hydrogels were used as wound dressing for wound healing. (B) Photographs of skin wounds on days 0, 5, 10 and 15 after the treatment using GelMA, ECM-G, PDA/ECM-G, and AC@PDA/ECM-G hydrogels, respectively, and gauze treatment was used as a blank group, and the corresponding wound healing trajectories were recorded. C) Wound area, (D) wound size, and (E) wound healing time were recorded after the treatment.

3.5 *In vivo* Wound Healing Evaluation

The in vitro results demonstrated that the prepared bioactive hydrogels based on decellularized ECM, GelMA, and AC@PDA nanoparticles are the potential as wound dressings for wound healing. Next, the performance of the obtained bioactive hydrogels as wound dressings was assessed using Sprague-Dawley (SD) rat model

573 with the circular full-thickness excision wound (15 mm diameter) on the dorsal skin.
574 After the skin model was formed, subsequent treatments consisting of gauze (blank
575 group), GelMA, ECM-G, PDA/ECM-G, and AC@PDA/ECM-G hydrogels were
576 assessed via observation and tissue collection on days 5, 10, and 15 (**Figure 5A**).
577 Macroscopically, all prepared hydrogels treated groups (GelMA, ECM-G,
578 PDA/ECM-G, and AC@PDA/ECM-G hydrogels) displayed faster wound healing
579 compared to the blank group (**Figure 5B**). On day 5, there was no significant healing
580 effect observed for gauze, and GelMA hydrogel treated groups. However, ECM-G,
581 PDA/ECM-G, and AC@PDA/ECM-G hydrogels treated groups displayed shrunk
582 wounds with visible edges, and scabs were not also observed. On day 10, the wounds
583 of all treated groups shrunk significantly, especially the AC@PDA/ECM-G hydrogel
584 treated group displayed the fasted healing effect. On day 15, there was still a large
585 wound area for gauze treated group, and wounds treated by GelMA, ECM-G, and
586 PDA/ECM-G hydrogels were basically healed with black scars still left. However, the
587 AC@PDA/ECM-G treated wound was completely healing without a scar. The
588 AC@PDA/ECM-G hydrogel treated group had a lower wound area of 13.53 μm^2 at
589 day 10 in comparison to that of the GelMA treated group (40.72 μm^2), ECM-G treated
590 group (21.88 μm^2), and PDA/ECM-G treated group (23.57 μm^2), and wound area of
591 AC@PDA/ECM-G hydrogel treated group was greatly decreased to 0.27 μm^2, which
592 was considered completely healed (**Figure 5C**). In addition, all prepared bioactive
593 hydrogel treated groups (ECM-G, PDA/ECM-G, and AC@PDA/ECM-G) displayed
594 smaller wound size than that of gauze and GelMA treated groups on days 5, 10, and

15 (**Figure 5D**). Also, all prepared bioactive hydrogels treated groups had a quicker wound healing rate than gauze and GelMA treated groups (**Figure 5E**), affirming that the bioactive hydrogels as wound dressings could effectively accelerate wound healing.

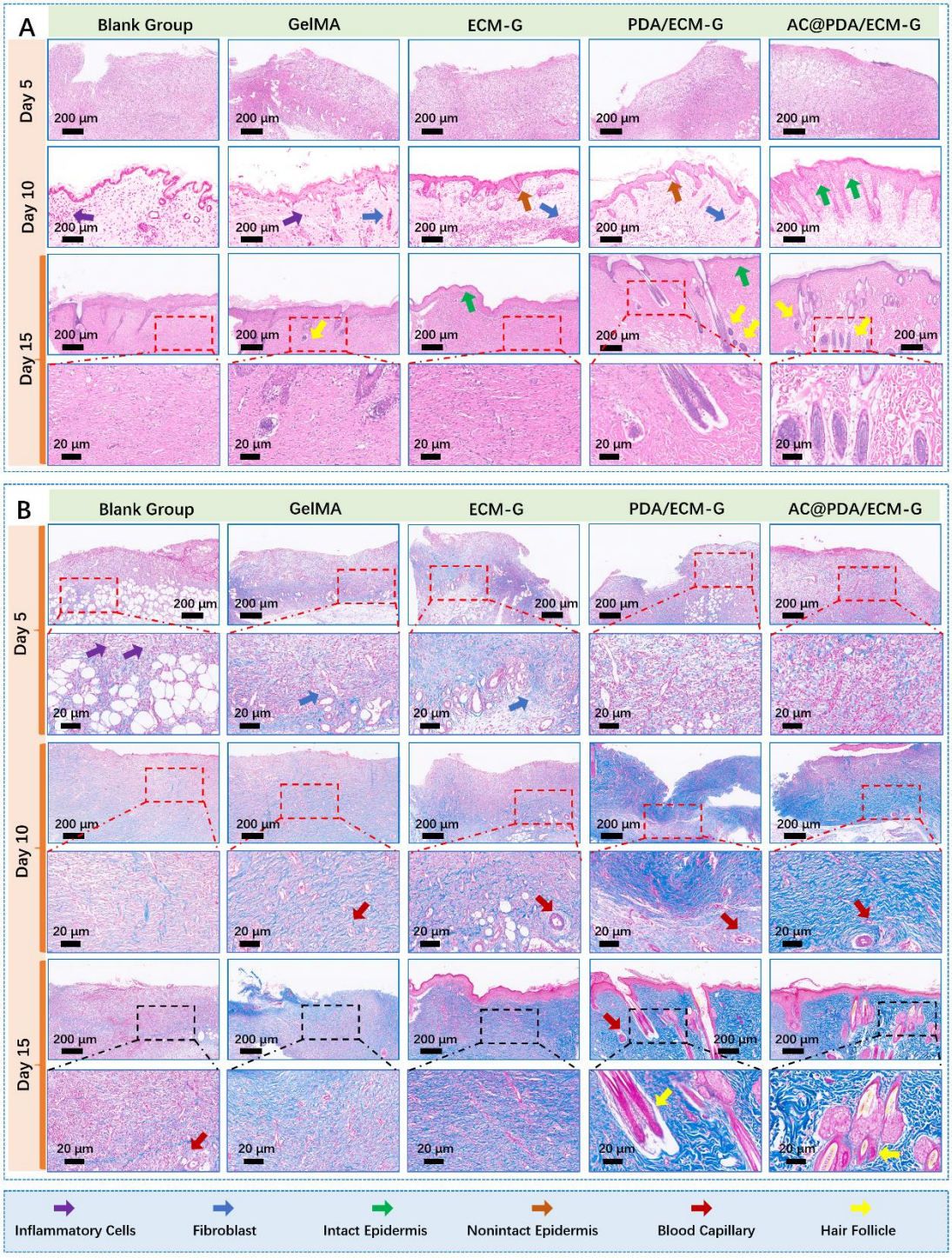

Figure 6. (A) H&E and (B) Masson's staining images of wound tissue on days 0, 5, 10 and 15 after the treatment using GelMA, ECM-G, PDA/ECM-G, and AC@PDA/ECM-G hydrogels, respectively, and gauze treatment was used as blank group.

3.6 *In vivo* Histological Analysis

The wound healing progression using bioactive hydrogels as wound dressings was assessed using histopathological evaluation. Results from histological analysis by H&E staining (**Figure 6A**) and Masson's staining (**Figure 6B**) were consistent with the wound healing rate (**Figure 5**). Wound healing is a common physiological process which process usually includes the hemostasis stage, inflammation stage, proliferation stage, and remodeling stage (**Figure 5A**) [65]. H&E and Masson's staining results displayed that the epidermal layers had not completely shaped after 15 days in the blank group and GelMA hydrogel treated group. According to the epithelium cell layer score (**Figure 7A**), ECM-based hydrogels (ECM-G, PDA/ECM-G, and AC@PDA/ECM-G) treated groups showed higher scores than the blank group and GelMA treated group on days 5, 10, and 15. The AC@PDA/ECM-G hydrogel treated group displayed the highest score on days 5 and 15, confirming that the epidermal layer was completely shaped. In addition, fibroblasts were observed in all groups, and the number of fibroblasts increased from day 5 to 15 (**Figure 7B**). Notably, the inflammatory cells were still infiltrated in the around tissue in the blank group on day 15. On day 5, a large number of inflammatory cells, such as lymphocytes and macrophages, migrated into the wound area for each group, which caused an

622 inflammatory response [66]. Apparently, more inflammatory cells were observed in
623 the blank group and GelMA hydrogel treated group than in ECM-based hydrogels
624 treated groups. The inflammatory cell score of each group was decreased from day 5
625 to 15, and ECM-based hydrogels treated groups displayed lower scores than other
626 groups (**Figure 7C**). In addition, the blood capillaries were apparently observed on
627 day 10, and the number of newly formed capillaries greatly increased from day 10 to
628 day 15 (**Figure 7D**). The AC@PDA/ECM-G hydrogel treated group displayed the
629 highest newly formed capillary number among all groups on days 5, 10, and 15. The
630 scabs were obviously observed from the H&E staining images in the blank group, and
631 GelMA hydrogel treated group on day 10. Instead, the epidermis, including the intact
632 epidermis and nonintact epidermis, for ECM-based hydrogels treated groups were
633 formed. The dermis formed in AC@PDA/ECM-G hydrogel treated group was thicker
634 than other groups (**Figure 7E**). The regenerated epidermis and dermis tissues are the
635 hallmarks of the fully healed wound in the middle and later stages of the wound
636 healing process [67].
637

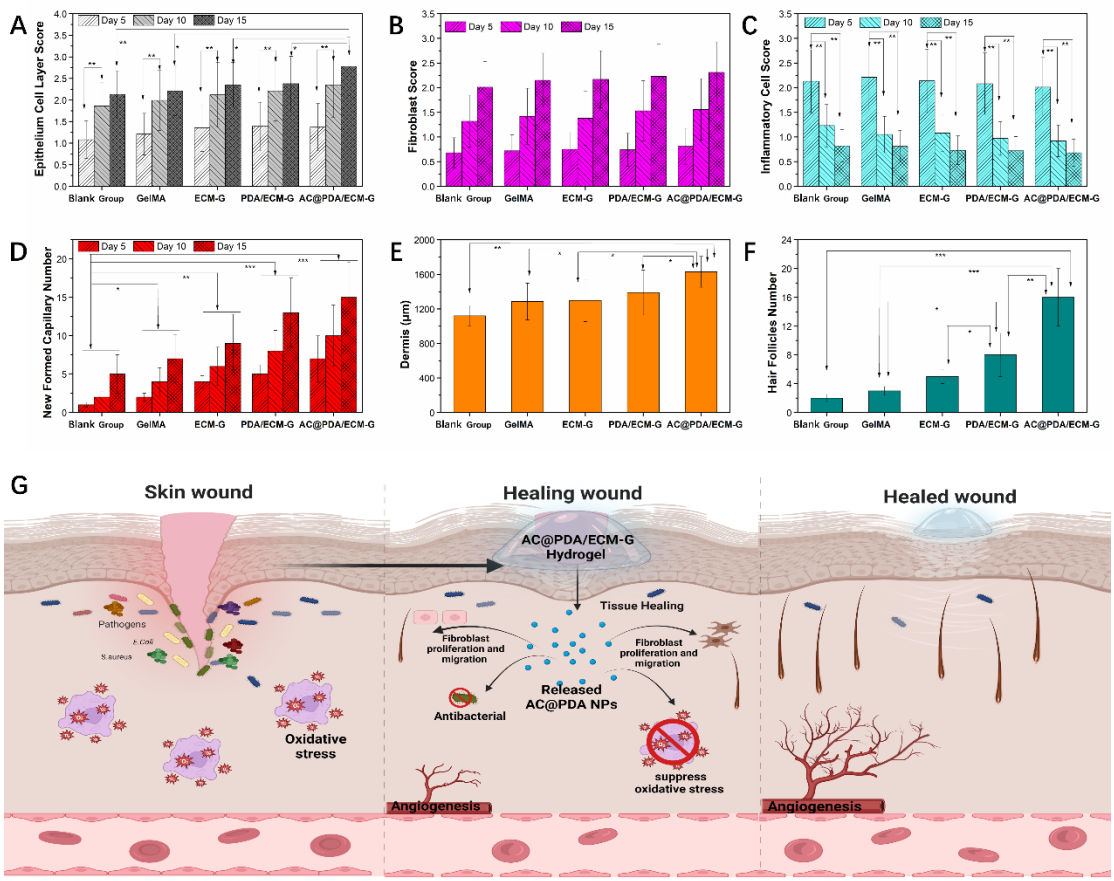

Figure 7. (A) Epithelium cell layer score, (B) fibroblast score, (C) inflammatory cell score, and (D) newly formed capillary number in each group after the treatment using gauze (blank group), GelMA, ECM-G, PDA/ECM-G, and AC@PDA/ECM-G hydrogels on day 5, 10 and 15. (E) The thickness of the dermis (μm) and (F) the number of hair follicles in each group on day 15. *$p < 0.05$, **$p < 0.01$, and ***$p < 0.001$. (G) Illustration of the mechanism of scarless wound healing using the fabricated bioactive AC@PDA/ECM-G hydrogel as a wound dressing.

The absence of secondary appendages in the regenerated tissues, such as hair follicles, causes the formation of scars, and also further causes mechanical and functional losses of the healed skin [43, 68, 69]. The number of hair follicles for each group was obtained from the whole sections on day 15, shown in Figure 7F. The

number of regenerated hair follicles in AC@PDA/ECM-G hydrogel treated group was greatly higher than that of other groups, implying that AC@PDA/ECM-G hydrogel could prevent the scarring propensity of skin, thus promoting full-thickness scarless wound healing efficiently. The proposed model of the wound healing mechanism of AC@PDA/ECM-G hydrogel is shown in Figure 7G. AC can remove ROS and prevent peroxidation damage at the wound site due to its high antioxidant activity via the upregulation of cellular antioxidant machinery thanks to its multiple phenolic hydroxyl groups [70, 71]. Moreover, the released asiaticoside from the AC@PDA/ECM-G can induce the proliferation and migration of fibroblast and keratinocytes via up-regulation of mitogen-activated protein kinase (MAPK) and transforming growth factor-beta 1 (TGF-β1) [72]. Furthermore, the active role of asiaticoside in promoting angiogenesis, new hair follicles, and new collagen synthesis, may effectively accelerate scarless skin regeneration [73].

4. Conclusion

This study presents a new method for the synthesis of AC@PDA nanoparticles and their incorporation into decellularized ECM and GelMA hydrogels to create bioactive composite hydrogels for use as wound dressings. The hydrogel was made using ECM, GelMA, and AC@PDA nanoparticles. The prepared hydrogels showed good mechanical properties, water absorption and retention, radical scavenging rate, rheological properties, and biodegradability. The *in vitro* results showed that the

prepared bioactive hydrogels were cytocompatible and enhanced cell migration, and the in vivo results demonstrated that the AC@PDA/ECM-G hydrogel had the best wound healing effect among the tested materials. The results suggest that the prepared bioactive hydrogels have great potential for use as wound dressings to promote wound healing ~~and avoid infection.~~ These results indicate that the AC@PDA/ECM-G hydrogel has the potential to be used as a wound dressing material.

Author Contribution

Shuang Liu: Methodology, Data curation, Writing- Original draft preparation. **Yingsong Zhao**: Formal analysis, Visualization, Investigation. **Ming Li***:* Software, Formal analysis, Writing- Reviewing and Editing. **Lei Nie:** Conceptualization, Methodology, Software, Formal analysis, Writing- Original draft preparation, Writing- Reviewing and Editing, Supervision. **Qianqian Wei**: Data curation, Software, Validation. **Okoro Oseweuba Valentine:** Writing- Reviewing and Editing. **Hafez Jafari**: Data curation, Software, Validation. **Siyuan Wang**: Software, Validation. **Jun Deng**: Software, Validation. **Jianghai Chen:** Writing- Reviewing and Editing. **Amin Shavandi:** Writing- Reviewing and Editing. **Lihong Fan**: Software, Validation, Supervision, Project administration, Funding acquisition, Writing- Reviewing and Editing.

Conflicts of Competing Interest

The authors declare no competing financial interest.

Acknowledgements

We thank Scientific Research Project of Sanya Yazhouwan Science and Technology City Administration Bureau (SKJC-2020-01-004), Open Fund Program of Sanya Science and Technology Park (2021KF0009), Open Fund Program of Sanya Science and Technology Park (2020KF0016), Science and Technology Innovation Special Project of Rizhao (2019CXZX1108). The authors acknowledge the help from Prof. Qiuju Zhou, Miss Zihe Jin, Dr. Zongwen Zhang, and Dr. Dongli Xu, in the Analysis & Testing Center of XYNU.

References

[1] S. Tavakoli, A.S. Klar, Advanced hydrogels as wound dressings, Biomolecules 10(8) (2020) 1169.
[2] M.F. Graça, S.P. Miguel, C.S. Cabral, I.J. Correia, Hyaluronic acid—Based wound dressings: A review, Carbohydrate polymers 241 (2020) 116364.
[3] Y. Liang, J. He, B. Guo, Functional hydrogels as wound dressing to enhance wound healing, Acs Nano 15(8) (2021) 12687-12722.
[4] S. Homaeigohar, A.R. Boccaccini, Antibacterial biohybrid nanofibers for wound dressings, Acta biomaterialia 107 (2020) 25-49.
[5] R. Dong, B. Guo, Smart wound dressings for wound healing, Nano Today 41 (2021) 101290.
[6] E.M. Ahmed, Hydrogel: Preparation, characterization, and applications: A review, Journal of advanced research 6(2) (2015) 105-121.
[7] V. Brumberg, T. Astrelina, T. Malivanova, A. Samoilov, Modern wound dressings: Hydrogel dressings, Biomedicines 9(9) (2021) 1235.
[8] L. Mao, L. Wang, M. Zhang, M.W. Ullah, L. Liu, W. Zhao, Y. Li, A.A.Q. Ahmed, H. Cheng, Z. Shi, In situ synthesized selenium nanoparticles-decorated bacterial cellulose/gelatin hydrogel with enhanced antibacterial, antioxidant, and anti-inflammatory capabilities for facilitating skin wound healing, Advanced healthcare materials 10(14) (2021) 2100402.
[9] L. Gao, Y. Zhou, J. Peng, C. Xu, Q. Xu, M. Xing, J. Chang, A novel dual-adhesive and bioactive hydrogel activated by bioglass for wound healing, NPG Asia Materials 11(1) (2019) 1-11.
[10] X. Zhang, X. Kang, L. Jin, J. Bai, W. Liu, Z. Wang, Stimulation of wound healing using bioinspired hydrogels with basic fibroblast growth factor (bFGF), International journal of nanomedicine 13 (2018) 3897.

[11] L. Kong, Z. Wu, H. Zhao, H. Cui, J. Shen, J. Chang, H. Li, Y. He, Bioactive injectable hydrogels containing desferrioxamine and bioglass for diabetic wound healing, ACS applied materials & interfaces 10(36) (2018) 30103-30114.
[12] M.T. Spang, K.L. Christman, Extracellular matrix hydrogel therapies: In vivo applications and development, Acta biomaterialia 68 (2018) 1-14.
[13] W. Zhang, A. Du, S. Liu, M. Lv, S. Chen, Research progress in decellularized extracellular matrix-derived hydrogels, Regenerative Therapy 18 (2021) 88-96.
[14] A.D. Theocharis, S.S. Skandalis, C. Gialeli, N.K. Karamanos, Extracellular matrix structure, Advanced drug delivery reviews 97 (2016) 4-27.
[15] C. Fuoco, L.L. Petrilli, S. Cannata, C. Gargioli, Matrix scaffolding for stem cell guidance toward skeletal muscle tissue engineering, Journal of orthopaedic surgery and research 11(1) (2016) 1-8.
[16] A.J. Sutherland, G.L. Converse, R.A. Hopkins, M.S. Detamore, The bioactivity of cartilage extracellular matrix in articular cartilage regeneration, Advanced healthcare materials 4(1) (2015) 29-39.
[17] C. Zhao, S. Wang, G. Wang, M. Su, L. Song, J. Chen, S. Fan, X. Lin, Preparation of decellularized biphasic hierarchical myotendinous junction extracellular matrix for muscle regeneration, Acta biomaterialia 68 (2018) 15-28.
[18] B.M. Sicari, V. Agrawal, B.F. Siu, C.J. Medberry, C.L. Dearth, N.J. Turner, S.F. Badylak, A murine model of volumetric muscle loss and a regenerative medicine approach for tissue replacement, Tissue Engineering Part A 18(19-20) (2012) 1941-1948.
[19] J.S. Choi, J.D. Kim, H.S. Yoon, Y.W. Cho, Full-thickness skin wound healing using human placenta-derived extracellular matrix containing bioactive molecules, Tissue Engineering Part A 19(3-4) (2013) 329-339.
[20] V. Ryzhuk, X.-x. Zeng, X. Wang, V. Melnychuk, L. Lankford, D. Farmer, A. Wang, Human amnion extracellular matrix derived bioactive hydrogel for cell delivery and tissue engineering, Materials science & engineering. C, Materials for biological applications 85 (2018) 191.
[21] V.A.S. David, V.R. Güiza-Argüello, M.L. Arango-Rodríguez, C.L. Sossa, S.M. Becerra-Bayona, Decellularized tissues for wound healing: towards closing the gap between scaffold design and effective extracellular matrix remodeling, Frontiers in Bioengineering and Biotechnology 10 (2022).
[22] W. Lin, X. Qi, W. Guo, D. Liang, H. Chen, B. Lin, X. Deng, A barrier against reactive oxygen species: chitosan/acellular dermal matrix scaffold enhances stem cell retention and improves cutaneous wound healing, Stem cell research & therapy 11(1) (2020) 1-17.
[23] K. Bankoti, A.P. Rameshbabu, S. Datta, P. Goswami, M. Roy, D. Das, S.K. Ghosh, A.K. Das, A. Mitra, S. Pal, Dual functionalized injectable hybrid extracellular matrix hydrogel for burn wounds, Biomacromolecules 22(2) (2020) 514-533.
[24] L.Y. Kerwin, A.K. El Tal, M.A. Stiff, T.M. Fakhouri, Scar prevention and remodeling: a review of the medical, surgical, topical and light treatment approaches, International journal of dermatology 53(8) (2014) 922-936.
[25] D. Kiritsi, A. Nyström, The role of TGFβ in wound healing pathologies, Mechanisms of ageing and development 172 (2018) 51-58.
[26] J. Zhang, Y. Zheng, J. Lee, J. Hua, S. Li, A. Panchamukhi, J. Yue, X. Gou, Z. Xia, L. Zhu, A pulsatile release platform based on photo-induced imine-crosslinking hydrogel promotes scarless wound healing, Nature communications 12(1) (2021) 1-13.

[27] F. Wu, D. Bian, Y. Xia, Z. Gong, Q. Tan, J. Chen, Y. Dai, Identification of major active ingredients responsible for burn wound healing of Centella asiatica herbs, Evidence-Based Complementary and Alternative Medicine 2012 (2012).
[28] R. Arora, R. Kumar, A. Agarwal, K. Reeta, Y. Gupta, Comparison of three different extracts of Centella asiatica for anti-amnesic, antioxidant and anticholinergic activities: in vitro and in vivo study, Biomedicine & Pharmacotherapy 105 (2018) 1344-1352.
[29] J.H. Park, I.J. Yeo, J.S. Jang, K.C. Kim, M.H. Park, H.P. Lee, S.-B. Han, J.T. Hong, Combination effect of titrated extract of Centella asiatica and astaxanthin in a mouse model of phthalic anhydride-induced atopic dermatitis, Allergy, Asthma & Immunology Research 11(4) (2019) 548-559.
[30] Y. Kimura, M. Sumiyoshi, K.-i. Samukawa, N. Satake, M. Sakanaka, Facilitating action of asiaticoside at low doses on burn wound repair and its mechanism, European Journal of Pharmacology 584(2-3) (2008) 415-423.
[31] S. Narisepalli, S.A. Salunkhe, D. Chitkara, A. Mittal, Asiaticoside polymeric nanoparticles for effective diabetic wound healing through increased collagen biosynthesis: In-vitro and in-vivo evaluation, International Journal of Pharmaceutics (2022) 122508.
[32] S. Anand, P.S. Rajinikanth, D.K. Arya, P. Pandey, R.K. Gupta, R. Sankhwar, K. Chidambaram, Multifunctional Biomimetic Nanofibrous Scaffold Loaded with Asiaticoside for Rapid Diabetic Wound Healing, Pharmaceutics 14(2) (2022) 273.
[33] L. Wang, D. Li, Y. Shen, F. Liu, Y. Zhou, H. Wu, Q. Liu, B. Deng, Preparation of Centella asiatica loaded gelatin/chitosan/nonwoven fabric composite hydrogel wound dressing with antibacterial property, International Journal of Biological Macromolecules 192 (2021) 350-359.
[34] C. Choipang, T. Buntum, P. Chuysinuan, S. Techasakul, P. Supaphol, O. Suwantong, Gelatin scaffolds loaded with asiaticoside/2-hydroxypropyl-β-cyclodextrin complex for use as wound dressings, Polymers for Advanced Technologies 32(3) (2021) 1187-1193.
[35] H. Li, Q. Peng, Y. Guo, X. Wang, L. Zhang, Preparation and in vitro and in vivo study of asiaticoside-loaded nanoemulsions and nanoemulsions-based gels for transdermal delivery, International Journal of Nanomedicine 15 (2020) 3123.
[36] L. Liu, Z. Ding, Y. Yang, Z. Zhang, Q. Lu, D.L. Kaplan, Asiaticoside-laden silk nanofiber hydrogels to regulate inflammation and angiogenesis for scarless skin regeneration, Biomaterials Science 9(15) (2021) 5227-5236.
[37] F. Zhao, J. Cheng, J. Zhang, H. Yu, W. Dai, W. Yan, M. Sun, G. Ding, Q. Li, Q. Meng, Comparison of three different acidic solutions in tendon decellularized extracellular matrix bio-ink fabrication for 3D cell printing, Acta Biomaterialia 131 (2021) 262-275.
[38] H. Song, Z. Yin, T. Wu, Y. Li, X. Luo, M. Xu, L. Duan, J. Li, Enhanced effect of tendon stem/progenitor cells combined with tendon-derived decellularized extracellular matrix on tendon regeneration, Cell Transplantation 27(11) (2018) 1634-1643.
[39] Q. Wu, L. Wang, P. Ding, Y. Deng, O.V. Okoro, A. Shavandi, L. Nie, Mercaptolated chitosan/methacrylate gelatin composite hydrogel for potential wound healing applications, Composites Communications 35 (2022) 101344.
[40] K. Rahali, G. Ben Messaoud, C.J.F. Kahn, L. Sanchez-Gonzalez, M. Kaci, F. Cleymand, S. Fleutot, M. Linder, S. Desobry, E. Arab-Tehrany, Synthesis and Characterization of Nanofunctionalized Gelatin Methacrylate Hydrogels, Int J Mol Sci 18(12) (2017). https://doi.org/10.3390/ijms18122675.

[41] Z. Li, B. Wang, Q. Zhang, Y. Qu, H. Xu, G. Li, Preparation and antioxidant property of extract and semipurified fractions of Caulerpa racemosa, Journal of applied phycology 24(6) (2012) 1527-1536.
[42] S. Liu, Y. Zhao, H. Wei, L. Nie, P. Ding, H. Sun, Y. Guo, T. Chen, O.V. Okoro, A. Shavandi, Injectable hydrogels based on silk fibroin peptide grafted hydroxypropyl chitosan and oxidized microcrystalline cellulose for scarless wound healing, Colloids and Surfaces A: Physicochemical and Engineering Aspects (2022) 129062.
[43] Q. Bai, L. Teng, X. Zhang, C.M. Dong, Multifunctional Single-Component Polypeptide Hydrogels: The Gelation Mechanism, Superior Biocompatibility, High Performance Hemostasis, and Scarless Wound Healing, Advanced Healthcare Materials 11(6) (2022) 2101809.
[44] Y. Abramov, B. Golden, M. Sullivan, S.M. Botros, J.J.R. Miller, A. Alshahrour, R.P. Goldberg, P.K. Sand, Histologic characterization of vaginal vs. abdominal surgical wound healing in a rabbit model, Wound repair and regeneration 15(1) (2007) 80-86.
[45] S. Wang, Y. Wang, L. Song, J. Chen, Y. Ma, Y. Chen, S. Fan, M. Su, X. Lin, Decellularized tendon as a prospective scaffold for tendon repair, Materials Science and Engineering: C 77 (2017) 1290-1301.
[46] A.D. Eren, R. Sinha, E.D. Eren, Y. Huipin, S. Gulce-Iz, H. Valster, L. Moroni, J. Foolen, J. de Boer, Decellularized porcine achilles tendon induces anti-inflammatory macrophage phenotype in vitro and tendon repair in vivo, Journal of Immunology and Regenerative Medicine 8 (2020) 100027.
[47] Y. Tang, Y. Tan, K. Lin, M. Zhu, Research progress on polydopamine nanoparticles for tissue engineering, Frontiers in Chemistry 9 (2021).
[48] H. Zhao, Z. Zeng, L. Liu, J. Chen, H. Zhou, L. Huang, J. Huang, H. Xu, Y. Xu, Z. Chen, Polydopamine nanoparticles for the treatment of acute inflammation-induced injury, Nanoscale 10(15) (2018) 6981-6991.
[49] B. Poinard, S.Z.Y. Neo, E.L.L. Yeo, H.P.S. Heng, K.G. Neoh, J.C.Y. Kah, Polydopamine nanoparticles enhance drug release for combined photodynamic and photothermal therapy, ACS applied materials & interfaces 10(25) (2018) 21125-21136.
[50] H. Luo, C. Gu, W. Zheng, F. Dai, X. Wang, Z. Zheng, Facile synthesis of novel size-controlled antibacterial hybrid spheres using silver nanoparticles loaded with poly-dopamine spheres, Rsc Adv 5(18) (2015) 13470-13477.
[51] E. Lih, K.W. Park, S.Y. Chun, H. Kim, T.G. Kwon, Y.K. Joung, D.K. Han, Biomimetic porous PLGA scaffolds incorporating decellularized extracellular matrix for kidney tissue regeneration, ACS applied materials & interfaces 8(33) (2016) 21145-21154.
[52] F. Zhao, J. Cheng, M. Sun, H. Yu, N. Wu, Z. Li, J. Zhang, Q. Li, P. Yang, Q. Liu, Digestion degree is a key factor to regulate the printability of pure tendon decellularized extracellular matrix bio-ink in extrusion-based 3D cell printing, Biofabrication 12(4) (2020) 045011.
[53] M. Subaraja, A.J. Vanisree, The novel phytocomponent asiaticoside-D isolated from Centella asiatica exhibits monoamine oxidase-B inhibiting potential in the rotenone degenerated cerebral ganglions of Lumbricus terrestris, Phytomedicine 58 (2019) 152833.
[54] Y. Zhou, S.P. Petrova, K.J. Edgar, Chemical synthesis of polysaccharide–protein and polysaccharide–peptide conjugates: A review, Carbohydrate Polymers 274 (2021) 118662.
[55] R. Ahmad, S. Rizaldo, S.E. Shaner, D.S. Kissel, K.L. Stone, Immobilization of a Bienzymatic System via Crosslinking to a Metal-Organic Framework, Catalysts 12(9) (2022) 969.

[56] K. Chen, F. Wang, S. Liu, X. Wu, L. Xu, D. Zhang, In situ reduction of silver nanoparticles by sodium alginate to obtain silver-loaded composite wound dressing with enhanced mechanical and antimicrobial property, International Journal of Biological Macromolecules 148 (2020) 501-509.
[57] K. Kalantari, E. Mostafavi, B. Saleh, P. Soltantabar, T.J. Webster, Chitosan/PVA hydrogels incorporated with green synthesized cerium oxide nanoparticles for wound healing applications, European Polymer Journal 134 (2020) 109853.
[58] P. Hashim, H. Sidek, M.H.M. Helan, A. Sabery, U.D. Palanisamy, M. Ilham, Triterpene composition and bioactivities of Centella asiatica, Molecules 16(2) (2011) 1310-1322.
[59] P. Ding, Q. Wei, N. Tian, X. Ding, L. Wang, B. Wang, O.V. Okoro, A. Shavandi, L. Nie, Enzymatically crosslinked hydrogel based on tyramine modified gelatin and sialylated chitosan, Biomedical Materials (2022).
[60] L. Nie, J. Li, G. Lu, X. Wei, Y. Deng, S. Liu, S. Zhong, Q. Shi, R. Hou, Y. Sun, Temperature Responsive Hydrogel for Cells Encapsulation Based on Graphene Oxide Reinforced poly (N-isopropylacrylamide)/Hydroxyethyl-Chitosan, Mater Today Commun (2022) 103697.
[61] H. Hu, F.-J. Xu, Rational design and latest advances of polysaccharide-based hydrogels for wound healing, Biomaterials science 8(8) (2020) 2084-2101.
[62] F. Zheng, R. Li, Q. He, K. Koral, J. Tao, L. Fan, R. Xiang, J. Ma, N. Wang, Y. Yin, The electrostimulation and scar inhibition effect of chitosan/oxidized hydroxyethyl cellulose/reduced graphene oxide/asiaticoside liposome based hydrogel on peripheral nerve regeneration in vitro, Materials Science and Engineering: C 109 (2020) 110560.
[63] G. Guan, Q. Lv, S. Liu, Z. Jiang, C. Zhou, W. Liao, 3D-bioprinted peptide coupling patches for wound healing, Materials Today Bio 13 (2022) 100188.
[64] P.A. Shiekh, A. Singh, A. Kumar, Exosome laden oxygen releasing antioxidant and antibacterial cryogel wound dressing OxOBand alleviate diabetic and infectious wound healing, Biomaterials 249 (2020) 120020.
[65] F. Fan, S. Saha, D. Hanjaya-Putra, Biomimetic hydrogels to promote wound healing, Frontiers in Bioengineering and Biotechnology 9 (2021) 718377.
[66] L. Nie, P. Zou, S. Feng, J. Suo, Temperature-sensitive star-shaped block copolymers hydrogels for an injection application: Phase transition behavior and biocompatibility, Journal of Materials Science: Materials in Medicine 24(3) (2013) 689-700.
[67] S.A. Eming, P. Martin, M. Tomic-Canic, Wound repair and regeneration: mechanisms, signaling, and translation, Science translational medicine 6(265) (2014) 265sr6-265sr6.
[68] M. Hosseini, A. Shafiee, Engineering bioactive scaffolds for skin regeneration, Small 17(41) (2021) 2101384.
[69] S. Mascharak, H.E. desJardins-Park, M.F. Davitt, M. Griffin, M.R. Borrelli, A.L. Moore, K. Chen, B. Duoto, M. Chinta, D.S. Foster, Preventing Engrailed-1 activation in fibroblasts yields wound regeneration without scarring, Science 372(6540) (2021) eaba2374.
[70] R. Bahramsoltani, M.H. Farzaei, R. Rahimi, Medicinal plants and their natural components as future drugs for the treatment of burn wounds: an integrative review, Archives of dermatological research 306 (2014) 601-617.
[71] V. Buranasudja, D. Rani, A. Malla, K. Kobtrakul, S. Vimolmangkang, Insights into antioxidant activities and anti-skin-aging potential of callus extract from Centella asiatica (L.), Scientific Reports 11(1) (2021) 1-16.

[72] T. Unahabhokha, A. Sucontphunt, U. Nimmannit, P. Chanvorachote, N. Yongsanguanchai, V. Pongrakhananon, Molecular signalings in keloid disease and current therapeutic approaches from natural based compounds, Pharmaceutical Biology 53(3) (2015) 457-463.
[73] X. Nie, H. Zhang, X. Shi, J. Zhao, Y. Chen, F. Wu, J. Yang, X. Li, Asiaticoside nitric oxide gel accelerates diabetic cutaneous ulcers healing by activating Wnt/β-catenin signaling pathway, International Immunopharmacology 79 (2020) 106109.